Applied Catalysis B: Environmental 305 (2022) 121081

Contents lists available at ScienceDirect

Applied Catalysis B: Environmental

journal homepage: www.elsevier.com/locate/apcatb

Bulk and surface dual modification of nickel-cobalt spinel with ruthenium toward highly efficient overall water splitting

Dewen Wang [a,b,1], Yuting Chen [a,b,1], Libing Fan [a,c], Ting Xiao [a,b], Tian Meng [a,b], Zhicai Xing [a,*], Xiurong Yang [a,b,**]

[a] State Key Laboratory of Electroanalytical Chemistry, Changchun Institute of Applied Chemistry, Chinese Academy of Sciences, Changchun 130022, PR China
[b] University of Science and Technology of China, Hefei 230026, PR China
[c] College of Chemistry, Jilin University, Changchun 130012, PR China

ARTICLE INFO

Keywords:
Electrocatalysis
Overall water splitting
Nickel-cobalt spinel
Bulk and surface dual modification
High current density

ABSTRACT

The development of highly active and stable bifunctional catalysts toward overall water splitting at large current densities through delicate control of composition and structure is a challenging work. Herein, we combined the Ru-doping of $NiCo_2O_4$ spinel (NCO) and the surface modification with Ru nanoparticles through rational design and controllable fabrication (NCRO) as a dual modification method to markedly enhance the overall water splitting. Benefiting from the structure advantages, the synergistic electronic effects and optimal binding strength of the reaction intermediates, the NCRO exhibited excellent performance for both hydrogen evolution reaction and oxygen evolution reaction in alkaline media. The density functional theory calculations suggest that the dual modification could enhanced water dissociation ability, optimized the adsorption energy of reaction intermediates and altered the energy level of the *d* band center.

1. Introduction

Developing renewable and eco-friendly energy sources like tidal and solar energy is essential to our society due to the sharp deterioration of the environment caused by the excessive use of fossil fuels [1,2], while the intermittent nature of these energy sources impedes their continuous electric energy supply. The conversion of chemical energy stored by hydrogen fuel into electricity is an effective approach to solve this critical issue [3–5]. Meanwhile, the ever-decreasing electricity prices (average 6.41 cents/kwh for industrial electricity in the United States on Apr 2020, U.S. Energy Information Administration) have stimulated scientific researchers to explore electrocatalysts for the production of hydrogen from water electrolysis [6–8]. Among the current industrial electrolysis systems, alkaline electrolysis is most advanced due to the safety and long lifetimes [9]. However, overall water splitting composed of two half reactions, namely hydrogen evolution reaction (HER) and oxygen evolution reaction (OER), is thermodynamically unfavorable process that restricted by the high intrinsic activation barriers [10–13]. The efficiency of an alkaline electrolysis stack is only 63–71%$_{LHV}$ owing to the high overpotential in two half reactions, and industrial alkaline electrolyzers usually suffer from low operational current densities (<500 mA cm^{-2}) [14,15]. Whereas at practical condition, it is very attractive to develop bifunctional electrocatalyst for both cathode and anode because of the all-in-one convenience for membrane electrode fabrication [16,17]. Thus, exploring electrocatalysts with highly intrinsic activity, alkali resistance and long life, while at the same time affording the compatibility between cathode and anode will be the principle for design next-generation water splitting catalysts [18].

$NiCo_2O_4$ (NCO) spinel, which belongs to an inverse spinel structure (space group $Fd\bar{3}m$), is a kind of promising OER electrode material because of its intrinsic high activity, easy availability and anti-corrosion ability [19–21]. In the inverse structure, Ni occupying the octahedral (Oh) sites, whereas the Co staying in both Oh sites and tetrahedral (Td) sites, the mixed redox couples of Co^{3+} and Co^{2+}, Ni^{3+} and Ni^{2+} coexist in NCO [22–24]. To improve its OER performance, many methods such as tuning composition/structures [25], controlling valence [22] and

* Corresponding author.
** Corresponding author at: State Key Laboratory of Electroanalytical Chemistry, Changchun Institute of Applied Chemistry, Chinese Academy of Sciences, Changchun 130022, PR China
E-mail addresses: xingzc@ciac.ac.cn (Z. Xing), xryang@ciac.ac.cn (X. Yang).
[1] These authors contributed equally to this work.

https://doi.org/10.1016/j.apcatb.2022.121081
Received 27 September 2021; Received in revised form 24 November 2021; Accepted 4 January 2022
Available online 6 January 2022

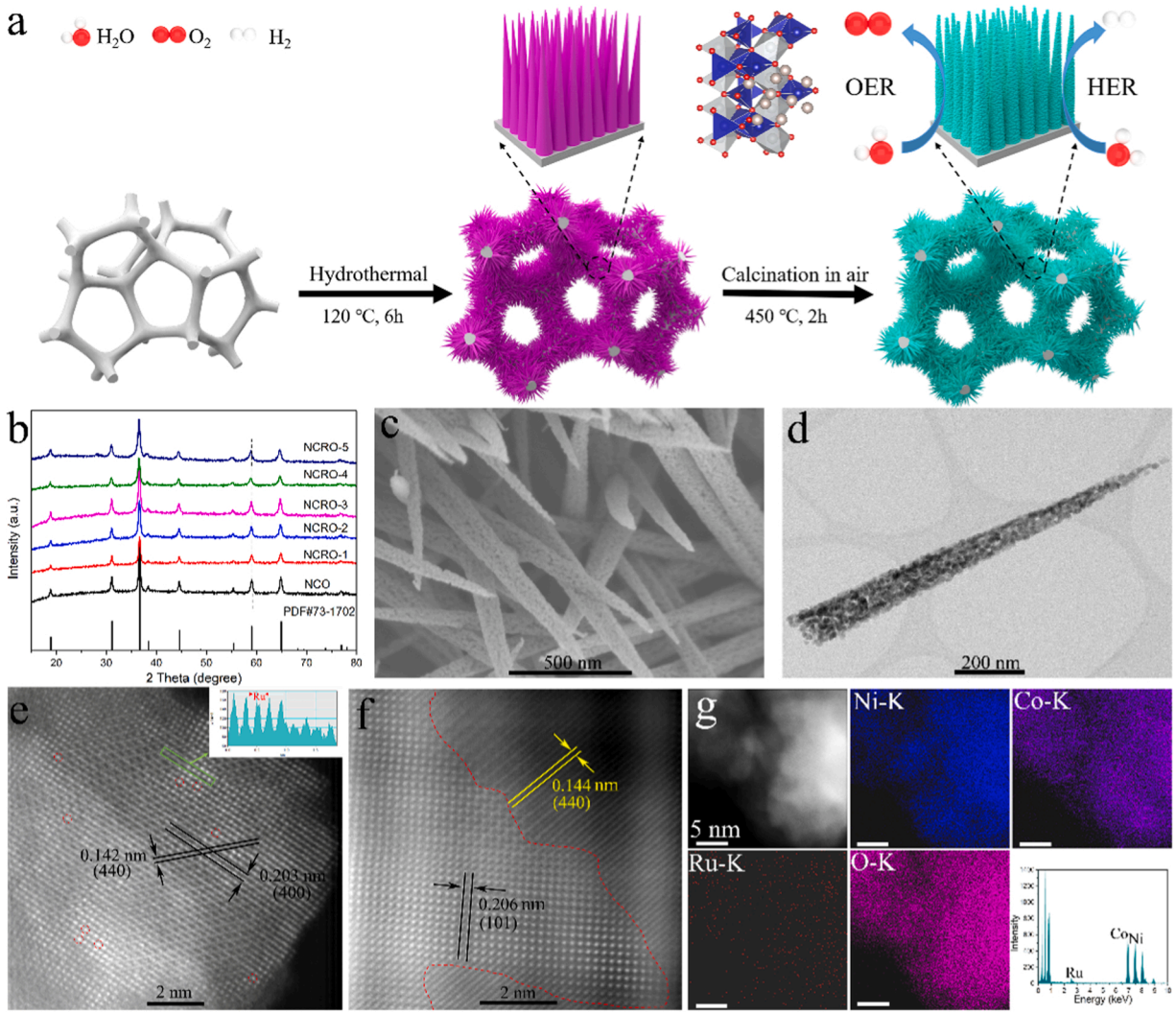

Fig. 1. (a) Schematic illustration of the preparation of NCRO. (b) XRD patterns of the as-prepared materials. (c) SEM and (d)TEM images of NCRO-4. (e) High-resolution HAADF-STEM image, contour plot for the marked region, and intensity profile along line shows the Ru sites that have stronger intensity. (f) High-resolution HAADF-STEM image of NCRO-4 with its surface was modified by Ru nanoparticles. (g) HAADF-STEM image, EDX elemental mapping images of Ni, Co, Ru, O and EDX spectrum for NCRO-4 nanowire.

creating defects [26] have been proposed. However, owing to the inherent complexity related to cation mixing, rare works have systematically studied the intrinsic kinetics of NCO for OER, and a few of them are able to achieve a high current density (>1000 mA cm^{-2}). As far as we know, NCO or even spinel family can rarely be used as bifunctional for both HER and OER, so it is a big challenge to simultaneously improve the HER and OER performance of NCO. As mentioned, the cations in NCO occupy different sites and have complex valence state, the substitution of these cations may cause unexpected effects. It is reported that introducing other noble metals can tremendously increase the number of active sites and produce complementary effects, so the idea of utilizing Ru as dopant come into being [27]. RuO_2 is the state-of-the-art OER catalyst currently, besides, Ru is a promising candidate for Pt in HER because it has a similar hydrogen bonding energy (≈65 Kcal mol^{-1} for Ru and ≈70 Kcal mol^{-1} for Pt) and the price is only a quarter of Pt, however, individual Ru nanomaterials cannot perform the satisfactory electrocatalytic activity [28–30]. Since the Ru suffer from weak water-dissociation ability (Volmer step: $H_2O + e^- + Cat \rightarrow Cat\text{-}H_{ads} + OH^-$, where Cat represents the catalyst and H_{ads} is adsorbed H), which seriously limiting the rate of HER in alkaline media [31,32]. Ni and Co-based catalysts have optimum Cat-OH bond strength which is beneficial to the adsorption of intermediate in Volmer step. Moreover, the hydrogen bonding energy of Ni and Co are weak, whereas Ru can strongly bind H [8,33–36]. The research work from Sun group proved that the strong synergetic electron coupling between single atomic noble metal and substrate can boost the OER activity and stability due to the optimal adsorption free energy of *OOH [35]. The Ru-loaded nickel hydroxide ultrathin nanoribbons synthesized by Chen et al. exhibited high efficient HER in alkaline media by taking the advantage of the synergy between atomic Ru and the nanoribbon morphology [36]. Therefore, the combination of Ru and NCO can not only accelerate water dissociation to H_{ads} but also promote the combination of H_{ads} to H_2 caused by effective synergistic effect. Ultimately, a theoretically excellent electrocatalyst could be constructed.

To verify the validity of our hypothesis, we used an industrially compatible method (A simple hydrothermal reaction followed by calcination in air) to efficiently combine NCO with different amounts of Ru (NCRO) as a bifunctional electrocatalyst. Initially, Ru doped into the lattice of bulk NCO and partially substituted Co_{Oh}, which affected the atomic coordination and electronic environment of bulk NCO. With the content increases, a part of Ru appears as metal nanoparticles on the NCO surface, and the conductivity of the material increases accordingly. The ratio of lattice Ru and metallic Ru is demonstrated by X-ray absorption spectroscopy, the atomic and electronic structure changes with

Ru contents are also analyzed. The optimal NCRO-4 electrode exhibits excellent overall water splitting performance in alkaline media. It requires the HER overpotential of only 18 and 138 mV to afford the current density of 10 and 1000 mA cm^{-2}, respectively, and the Tafel slope is 22 mV dec^{-1}. Moreover, the catalyst also shows an impressive OER performance that achieves the current density of 1500 mA cm^{-2} at overpotential of 420 mV. When it was used as both cathode and anode in an alkaline electrolytic cell, a low cell voltage of 1.45 V is needed to yield 10 mA cm^{-2} for overall water splitting. Furthermore, density functional theory (DFT) theoretical calculations reveal that the enhanced water dissociation ability and optimized adsorption energy of reaction intermediates are the crucial factors for extraordinary electrocatalytic activity. The proposed NCRO electrocatalyst can be generalized to the bulk and surface dual modification of spinel-based electrode for high current density water splitting.

2. Experimental section

2.1. Preparation of NCO and NCRO

NCO nanowire arrays were grown on Ni foam via a two-step method. To remove the oxide layer on the surface, a piece of Ni form (2 cm × 6 cm) was put into HCl solution about 10 min with ultrasonic cleaning and then cleaned several times by using deionized water. Then, 4 mmol of $NiCl_2{\cdot}6H_2O$, 8 mmol of $CoCl_2{\cdot}6H_2O$ and 15 mmol of urea were dissolved in 75 mL deionized water and stirred for 30 min under magnetic stirring. Subsequently, the cleaned Ni foam and the mixed solution were transferred into a 100 mL Teflon-lined stainless steel autoclave and heated to 120 °C for 6 h. After cooled to room temperature, the NCO precursor was obtained by cleaning several times with deionized water and drying in an oven at 60 °C. In the second step, the NCO precursor was calcined at 450 °C in a quartz tube for 2 h with the heating speed of 1 °C/min to get well defined crystallized NCO on Ni foam. The synthesis process of NCRO was consistent with that of NCO with the exception of the addition of $RuCl_3{\cdot}xH_2O$. NCRO with different Ru contents was prepared by changing the feed dosages of $RuCl_3{\cdot}xH_2O$. The product was labeled as sample 1–5, respectively, according to the different Ru concentrations (0.4, 0.8, 1.2, 1.6 and 2 mmol). The mass loading of NCRO-4 was 3.98 mg cm^{-2}.

2.2. Electrochemical measurements

a CHI660e electrochemical analyzer was used to evaluate the electrocatalytic performance. NCO and NCRO grown on Ni foam were directly used as the working electrode, a graphite rod was used as the counter electrode and a Hg/HgO electrode was used as the reference electrode. The ohmic potential (*iR*) drop losses from the solution resistance was subtracted from the following equation: $E_{RHE} = E_{Hg/HgO} + 0.098\ V + 0.059\ pH\text{-}iR$. Tafel slopes was conducted according to the equation ($\eta = a + b\ log j$) through the LSV curves. The stability tests of NCRO-4 were evaluated using cyclic voltammetry (CV) scanning and chronopotentiometry test. The double layer capacitance (C_{dl}) values were evaluated by cyclic voltammetry between 0.15 V and 0.35 V vs RHE with different scanning rates, where the current response caused by the double-layer charging.

3. Results and discussion

3.1. Catalysts characterization

The NCRO electrode was synthesize by a facile two-step procedure as schematically illustrated in Fig. 1**a**. The crystal structures of the synthesized NCO and NCRO were confirmed by XRD analysis (Fig. 1b). The identified diffraction peaks can be ascribed to the pure cubic phase of NCO (JCPDS card No. 73−1702) without detectable impurity peaks [37], indicating that the low content, highly dispersed and small Ru nanoparticles are difficult to be detected [28,38]. With the increased amounts of Ru replacing Co, a gradual peak shift to lower angles can be observed due to the different ionic radius of Ru and Co elements [6,39]. The morphology of the as-obtained materials was examined with SEM. Fig. S1 shows the SEM images of the NCO precursor, which clearly display the uniformly distributed nanowires array with smooth surface on Ni foam. After annealing conversion into spinel NCO, the nanowire morphology and the array feature are reserved completely, however, the enlarge view indicates that the nanowires become porous structures and which are composed of closely connected nanoparticles (Figs. S2 and S3a). The TEM and HAADF-STEM (Fig. S3) images indicate the porous structure and the lattice spacing of NCO. Moreover, the corresponding EDX elemental mapping images of NCO nanowire (Fig. S4) illustrate uniform distribution of Co, Ni and O element. With the addition of Ru, the morphology of NCRO (Fig. 1c, d, and Fig. S5) is similar as that of NCO (Figs. S2-S4), but the nanowires will agglomerate into grid-like nanosheet structure at the high Ru content (Fig. S6). As demonstrated in the Table S1, the Ru and Co contents of NCRO samples are quantitatively studied by inductively coupled plasma-optical emission spectrometry (ICP-OES). The specific surface areas of NCO, NCRO-1, NCRO-2, NCRO-3, NCRO-4, and NCRO-5 determined by nitrogen isothermal adsorption-desorption measurements are 124.2, 84.9, 95.2, 123.5, 130.1, and 113.7 $m^2\ g^{-1}$, respectively (Figs. S7 and S8). The mesoporous structure of NCO and NCRO is confirmed by the pore size distribution calculations. Compared with NCO, the ratio of pore size around 4.3 nm in NCRO-4 has increased, which lead to the larger specific surface area and rapid charge transfer process because of the shorten ions diffusion paths.

The structure of NCRO-4 was further elucidated by TEM and HAADF-STEM as it exhibited the best catalytic performance. As shown in Fig. 1d, NCRO-4 nanowire still maintained the porous structure that composed of closely connected nanoparticles. Fig. 1e and f show that the atomic HAADF-STEM images for the bulk doping and surface modification of NCRO-4, respectively. Fig. 1e shows that two sets of planes and their lattice spacings are 0.142 and 0.203 nm, in accordance with the standard crystal plane of (440) and (400) in cubic NCRO. The brighter sites labeled with round cycles and green rectangle represent the doped Ru atoms in the lattice (Fig. 1e), which have higher intensity in the intensity profile along line (inset in Fig. 1e) [40]. Two different crystal structures are present in Fig. 1f. The crystal plane marked by red dashed line is uniform and the lattice spacing is 0.206 nm which is corresponding to the (101) facet of Ru. The other crystal plane spacing of 0.144 nm can be assignable to (440) facets of NCRO. The result indicates that there are Ru nanoparticles attached to the NCRO surface. The HAADF-STEM and corresponding EDX elemental mappings/spectra proving that the Ni, Co, Ru and O atoms were uniformly distributed over whole nanowire (Fig. 1g). There was no agglomeration of Ru species into large particles in TEM and HAADF-STEM mapping images, testifying that the NCRO substrate was able to effectively anchor the supported Ru metal and keep a highly dispersed geometry of Ru domains.

The elemental composition and oxidation state of NCO and NCRO are further characterized by XPS. The high-resolution Ni 2p spectrum of the samples (Fig. S9) can be deconvolve into two spin-orbit peaks, characteristic of Ni^{2+} at 853.5 eV and Ni^{3+} at 855.1 eV, and two shakeup satellites [41]. Co 2p spectra can also be fitted into Co^{3+} at 779.6 eV and Co^{2+} at 781.1 eV (Fig. S10). The results confirmed that the elemental composition of NCO and NCRO contain Ni^{3+}, Ni^{2+}, Co^{3+} and Co^{2+} [42]. For the Ru 3p XPS spectra in NCRO (Fig. S11), the peaks appearing at 462.2 eV and 463.9 eV represent Ru^0 and Ru^{4+}, respectively [43,44]. The proportion of Ru^0 peak becomes larger as the Ru content increases, indicating more Ru nanoparticles will appear on the surface of NCRO. With regard to the O 1 s spectra (Fig. S12), the peak located at 529.4 eV can be attributed to metal-oxygen bonds, and the peak observed at 531.0 eV originates from contaminants, defects, and some surface species including hydroxyls, chemisorbed oxygen, unsaturated coordinated lattice oxygen, or substances inherent to the spinel

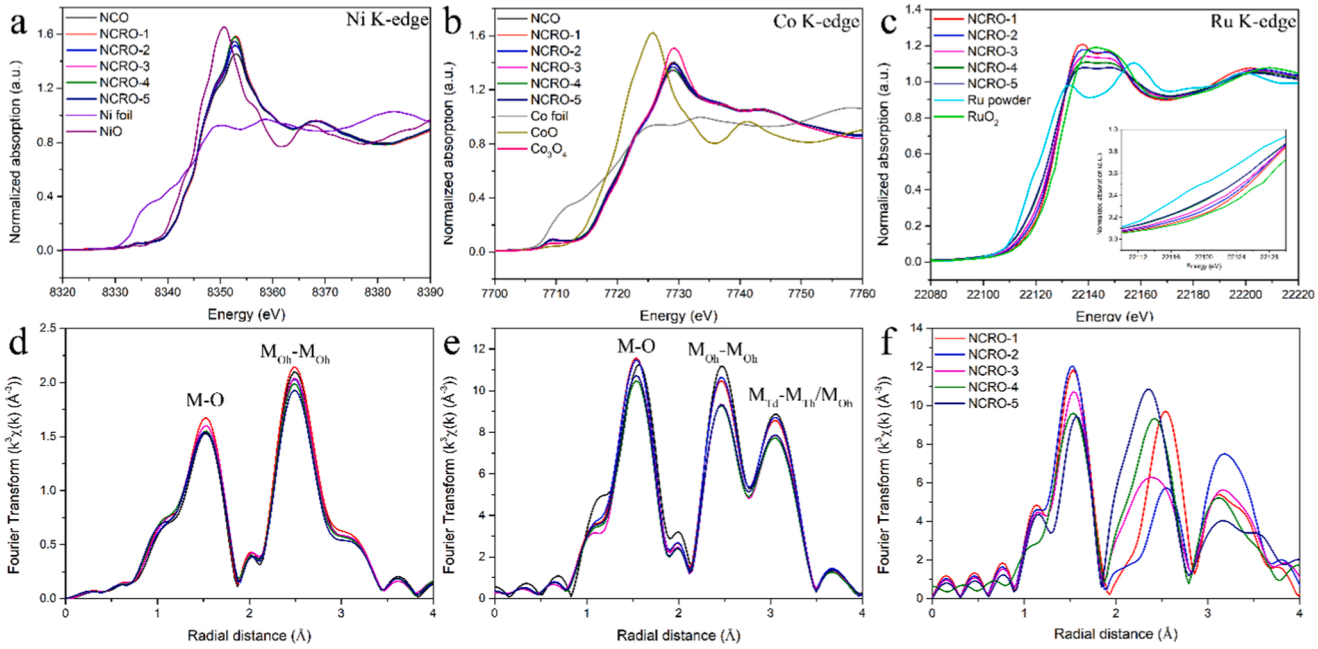

Fig. 2. (a) Ni, (b) Co and (c) Ru K-edge XANES spectra of NCO, various NCRO and standard samples. EXAFS k3χ(R) spectra of NCRO samples at (d) Ni, (e) Co and (f) Ru K-edge.

surface. Besides, the other peak obtained at 532.5 eV is typical of physically and chemically adsorbed water [45,46]. In addition, the comparison of Ni and Co spectra (Figs. S9 and S10) revealed that the binding energies of both Ni and Co for NCRO have obvious negative shifts compared to that of NCO, indicating the synergistic electronic interactions among Ni, Co and Ru [6,35,36].

The valency and site occupation of Ni, Co and Ru in spinel oxides are deeply analyzed by XANES and EXAFS. As shown in Fig. 2**a** and b, the valency of Ni in NCO and NCRO is higher than that of NiO, and the valency of Co is similar with that of Co_3O_4, reconfirmed the coexistence of Ni^{3+}, Ni^{2+}, Co^{3+} and Co^{2+}. However, the K-edge positions of Ru in NCRO progressively shift and approach lower binding energies which are closer to that of Ru powder (Fig. 2c), manifesting the decrease in oxidation state of Ru cations and the increased Ru nanoparticles [38,47]. In cubic spinel, the shell peak at ≈ 1.5 Å corresponds to the single scattering of the closest neighboring crystal oxygen (TM-O bond distance) near the absorbing transition metal position. Besides, the peaks at ≈ 2.5 Å (TM_{Oh}-TM_{Oh}) and ≈ 3.0 Å (TM_{Td}-TM_{Td} or TM_{Td}-TM_{Oh}) can be ascribed to the scattering of the metal ion from the closest neighboring metal ion near the Oh or Td site [48]. From the Fourier transform (FT) of

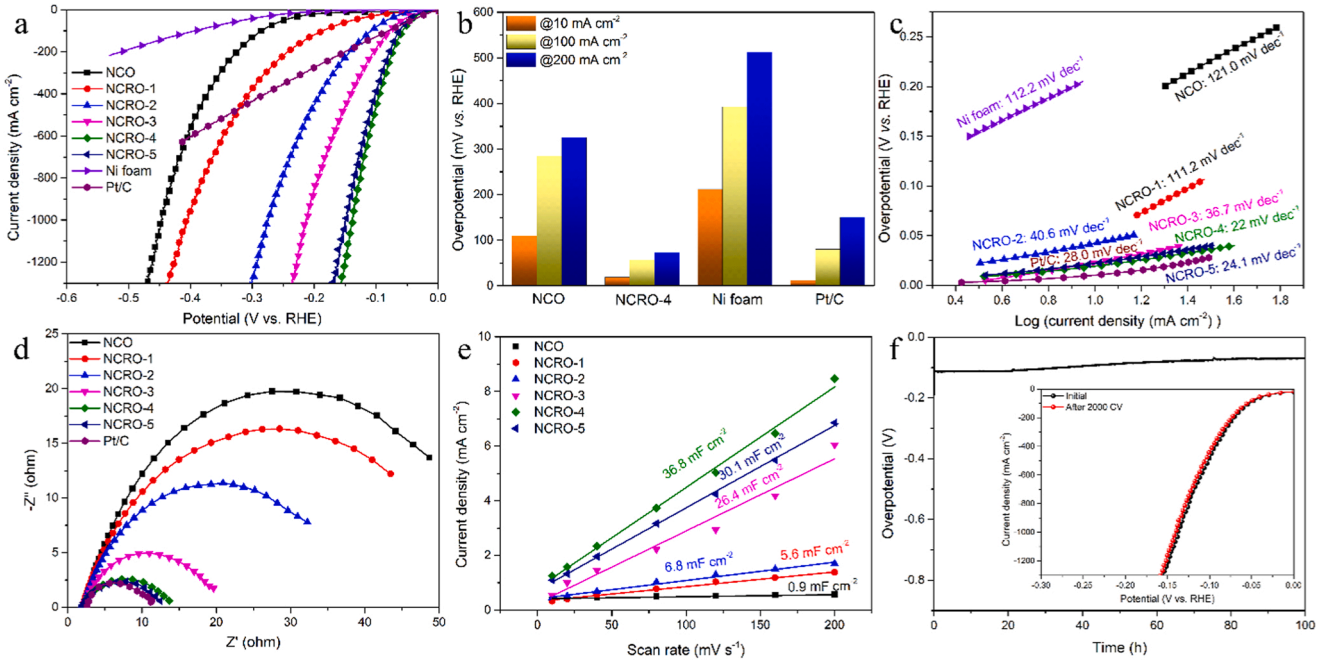

Fig. 3. Electrocatalytic activity for the HER. (a) The polarization curves, (b) histogram of overpotentials at different current densities, (c) Tafel plots of different electrocatalysts, (d) Nyquist plots (overpotential = 60 mV), and (e) the current density against scan rate of the as-obtained samples. (f) The chronopotentiometric curve of NCRO-4. Inset: LSV polarization curves of NCRO-4 before and after repeating 2000 CV scans.

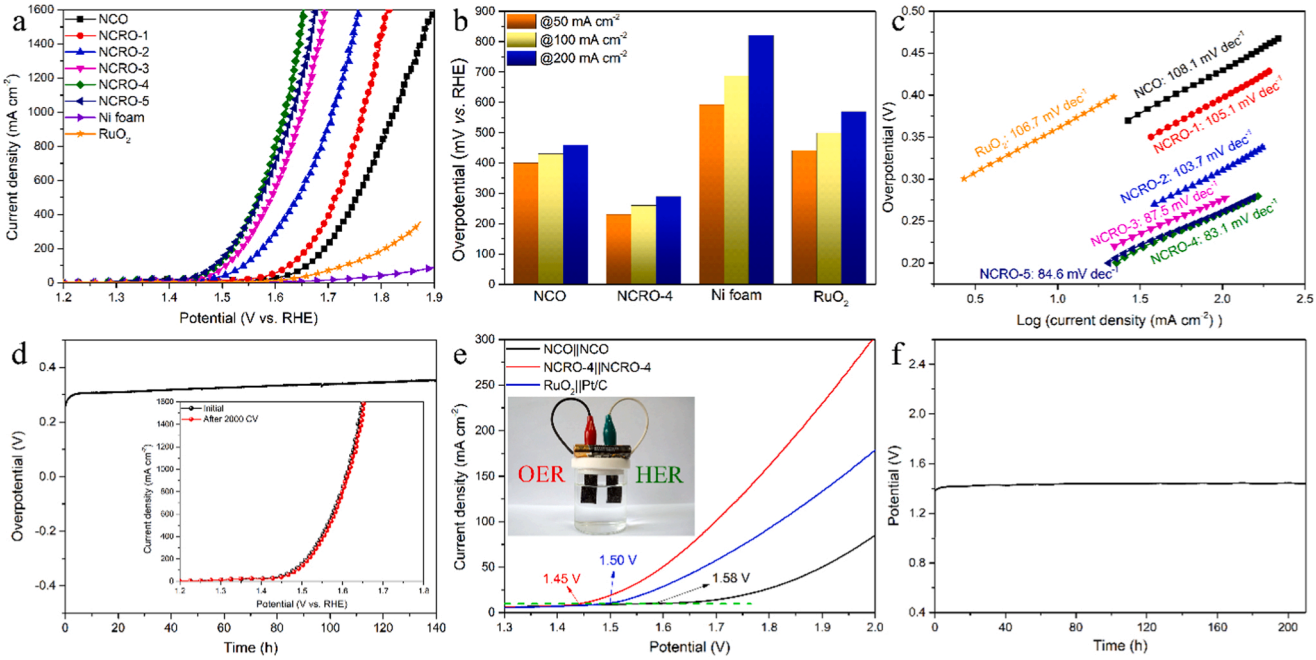

Fig. 4. Electrocatalytic activity for the OER. (a) The polarization curves, (b) histogram of overpotentials at different current densities, (c) Tafel plots of different electrocatalysts, and (d) the chronopotentiometric curve of NCRO-4. Inset: LSV polarization curves of NCRO-4 before and after repeating 2000 CV scans. (e) The polarization curves of NCO|| NCO, NCRO-4||NCRO-4 and RuO_2||Pt/C toward overall water splitting. The inset is the electrolyzer driven by a single-cell AAA battery. (f) The chronopotentiometric curve of NCRO-4||NCRO-4 at 10 mA cm^{-2}.

the absorption fine structure shown in Fig. 2d-f, Fig. S13, and Fig. S14, we find that the Ni K-edge spectra display only one TM_{Oh}-TM_{Oh} distance at ≈ 2.5 Å, whereas two atomic distances at ≈ 2.5 Å and ≈ 3.0 Å are observed for Co, confirming that the absorbing Ni atoms only occupy the Oh sites and the Co atoms occupy both Oh and Td sites, meanwhile, the EXAFS fitting results are shown in Fig. S15 and Table S2 [49]. Because the composition of Ru is relatively complex, we firstly analyze the data of NCRO-1. As shown in Fig. S16, the spectra of Ru in NCRO-1 is neither like that of RuO_2 or Ru powder, the peak at ≈ 2.5 Å indicates that the Ru occupy the Oh sites. Furthermore, the composition of Ru was analyzed using linear combination fitting method based on XANES spectra (Fig. S17 and Table S3), the results show that all the Ru doped into the lattice of NCRO-1. As the content increases, more Ru will exist in the form of Ru nanoparticles, which was in consistent with the results of ICP-OES (Table S1). The fitting results (Figs. S18 and S19, Tables S4 and S5) show the Ru-Ru coordination numbers (CN) of NCRO are smaller than that of Ru foil (CN=12), proving well dispersion of Ru nanoparticles on the surface [50]. Besides, the CN of Ru-Ru increases with the increase of Ru content in NRCO, indicating more and bigger Ru nanoparticles will appear on the surface.

3.2. Electrocatalytic activity toward HER

The HER activity of the samples was tested in 1 M KOH using a typical three-electrode system. As shown in Fig. 3**a** and b, NCO needs extremely high overpotentials of 109, 285 and 325 mV to achieve current densities of 10 (η_{10}), 100 (η_{100}) and 200 (η_{200}) mA cm^{-2}, respectively. The electrocatalytic performance of NCRO is gradually improved when Ru content is increased, but then decrease in the high Ru content, which can be attributed to the agglomeration of nanowires and the bigger nanoparticles of Ru metal. The NCRO-4 shows the best HER activity among all the samples (η_{10} =18 mV, η_{100} =57 mV and η_{200} =73 mV). It is worth mentioning that this performance is better than that of most reported electrocatalysts (see details in Table S6) include commercial Pt/C (η_{10} =11 mV, η_{100} =80 mV and η_{200} =150 mV). Furthermore, the HER performance of NCRO-4 is more outstanding in high current density. The overpotentials at 500 and 1000 mA cm^{-2} for NCRO-4 are only 103 and 138 mV, respectively, which are much smaller than that of Pt/C (η_{500} =400 mV). The Tafel plots derived from the corresponding LSV curves show that the Tafel slope of NCO is 121 mV dec^{-1} (Fig. 3c), suggesting that the rate determining step is the Volmer step [51]. Notably, the Tafel slope of NCRO-4 (22 mV dec^{-1}) is the lowest among the samples, implying that the HER process follows Volmer-Tafel mechanism, in which the Tafel step is the rate determining step [52]. The results demonstrate that the combination of Ru and NCO can decreased the energy barrier in the Volmer step thus accelerate H_2O dissociation. Furthermore, the intrinsic catalytic activity of each active site was reflected by the turnover frequency (TOF, Figs. S20 and S21). The TOF value of NCRO-4 is 1.22 s^{-1} at an overpotential of 100 mV, which is ≈ 147.0 and 4.9 times higher than that of NCO (0.0083 s^{-1}) and Pt/C (0.25 s^{-1}), respectively. As shown in Fig. 3d, the electrochemical impendence spectroscopy (EIS) indicates that the NCRO-4 has much smaller charge transfer resistance than that of NCO, suggesting the fastest electron transport. The conductivity of the materials become better with the increase of Ru content, and the resistances of NCRO-4 and NCRO-5 are similar with that of Pt/C. Furthermore, the electrochemically active surface area (ECSA) is proportional to C_{dl} (Fig. S22 and Fig. 3e), which is performed to estimate the number of active sites. The obtained C_{dl} value of NCRO-4 (36.8 mF cm^{-2}) is larger than that of NCO (0.9 mF cm^{-2}), suggesting the increased active sites for NCRO, which is beneficial to promote the conversion of more intermediate species to hydrogen on the surface. The electrocatalytic stability (especially in high current density) plays a vital role in assessing the practical applications of electrocatalyst. As shown in the inset of Fig. 3f, the polarization curve of NCRO-4 exhibits negligible differences after 2000 cyclic voltammetry (CV) scans. Furthermore, the NCRO-4 can maintain long-term stability over 100 h at the high current density of 300 mA cm^{-2} in electrolysis (Fig. 3f). The SEM images (Fig. S23) and XPS spectra (Fig. S24) of NCRO-4 after stability test demonstrated that the NCRO-4 possessed high structure robustness during HER process.

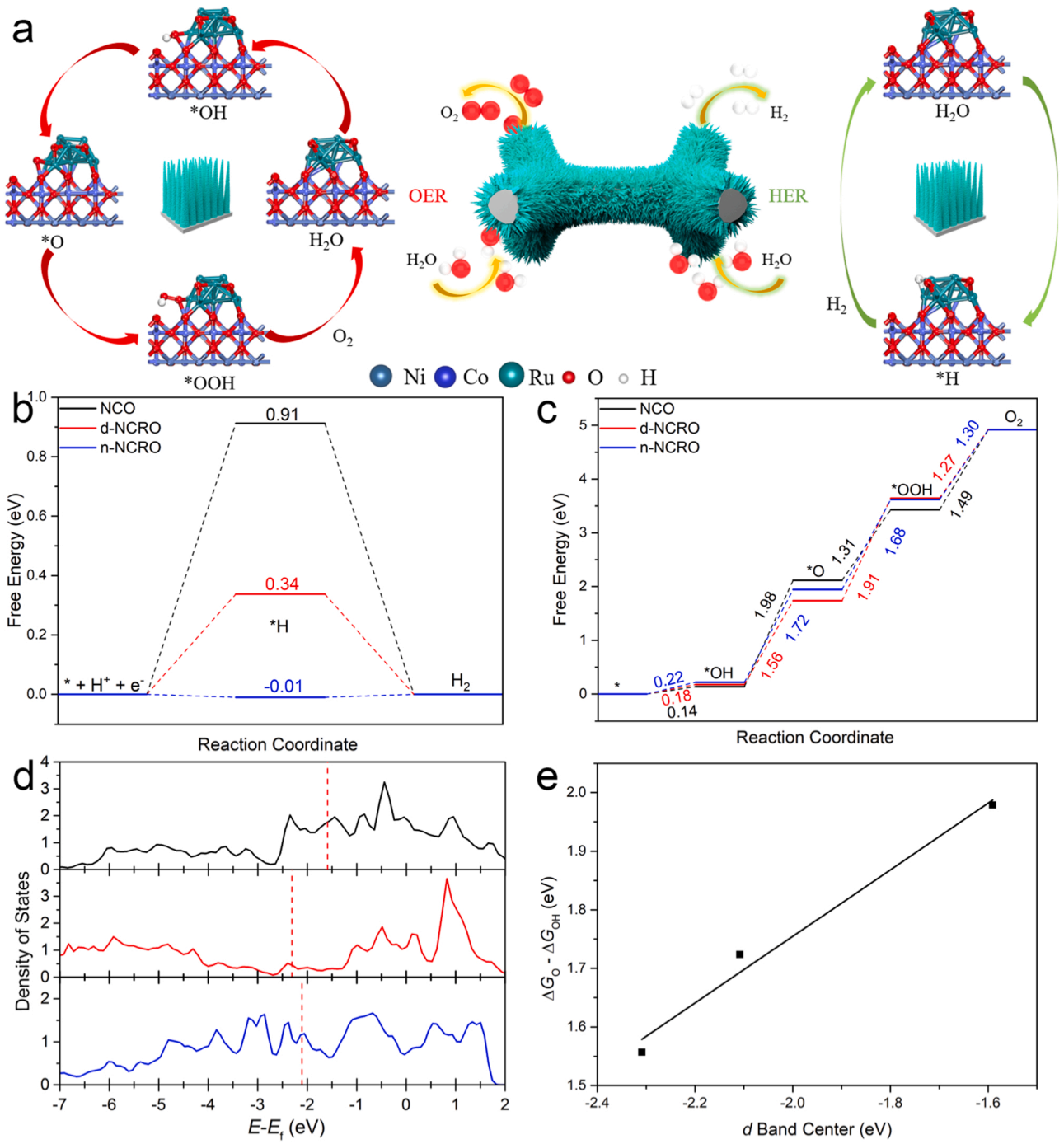

Fig. 5. (a) The atomic model of the samples, schematic of the whole HER and OER mechanism in the alkaline electrolyte. Free energy diagrams for (b) HER and (c) OER on NCO, d-NCRO and n-NCRO surfaces. (d) Density of states (DOS) of surface Co d orbitals of NCO and Ru d orbitals of d-NCRO and n-NCRO, where the red dashed lines represent the *d* band center. Fermi-level is set to zero. (e) linear relation of the as obtained date.

3.3. Electrocatalytic activity toward OER and overall water splitting

Following the HER test, the OER performance of the samples were also tested in 1 M KOH. As described in Fig. 4**a**, the NCRO-4 also displayed the best OER activity among all the samples with η_{50} of 230 mV, η_{100} of 260 mV and η_{200} of 290 mV, respectively, which outperformed that of NCO (η_{50} =400 mV, η_{100} =430 mV and η_{200} =460 mV) and RuO_2 (η_{50} =440 mV, η_{100} =500 mV and η_{200} =570 mV). Notably, NCRO-4 can attain the current density of 1600 mA cm^{-2} at only 420 mV. This activity is comparable or superior to many other electrodes reported previously (Table S7). Besides, the NCRO-4 also shows the smaller Tafel slope (83.1 mV dec^{-1}) than that of NCO (108.1 mV dec^{-1}), indicating the optimized kinetics during the OER process (Fig. 4c). Then, we also test the stability of NCRO-4 under alkaline solution (Fig. 4d). After 2000 CV cycles, the polarization curve exhibits neglectable decay, besides, the NCRO-4 can maintain 300 mA cm^{-2} over 140 h. Both SEM images (Fig. S25) and XPS spectra (Fig. S26) of NCRO-4 after the stability test verified that NCRO-4 had highly structural stability during long-term OER process. Encouraged by the excellent HER and OER performance, a two-electrode electrolyzer was fabricated using NCRO-4 as both cathode and anode toward overall water splitting (inset in Fig. 4e). As expected, NCRO-4 couple exhibits the best performance that only need

1.45 V cell voltage to deliver 10 mA cm^{-2}, this performance is much better than that of benchmark RuO_2||Pt/C couple (10 mA cm^{-2} at 1.50 V) and NCO couple (10 mA cm^{-2} at 1.58 V), as well as other reported electrocatalysts (Table S8). Surprisingly, a 1.50 V AAA battery was able to drive the NCRO-4 couple for overall water splitting with violent gas bubbles release (inset in Fig. 4e and Movie S1). Furthermore, the electrolytic cell exhibits excellent long-term stability that kept negligible change in the chronopotentiometric test over 200 h at 10 mA cm^{-2} (Fig. 4f) and showed a slight decrease in activity for over 200 h at large current density of 100 mA cm^{-2} (Fig. S27).

3.4. First-principles calculations

To further understand the role of Ru on the bulk and surface modification of NCO toward water splitting, theoretical investigations were performed based on DFT calculations. The atomic structures for the pure NCO, NCO with doped Ru atoms (d-NCRO) and Ru nanoparticles on the surface (n-NCRO) are show in Fig. 5**a** and Figs. S28-33. For HER, the efficiency of hydrogen generation was strongly associated with the free energy of *H (ΔG_{*H}). As shown in Fig. 5b, the calculated ΔG_{*H} is 0.91 eV for NCO, and 0.34 and − 0.01 eV for d-NCRO and n-NCRO, respectively, suggesting the more favorable *H adsorption kinetics of d-NCRO and n-NCRO during the HER process, especially n-NCRO. Refer to the previous conclusions, the combination of Ru and NCO can not only improve the Volmer process that optimize the water dissociation kinetics, but also accelerate the Tafel process that recombine H_{ads} to H_2. Then, the influences of Ru on NCO are also elucidated (Fig. 5c). The potential determining step (PDS) is the second step (*OH → *O) for NCO and n-NCRO and third step (*O → *OOH) for d-NCRO. The calculated free energy for the PDS is 1.98, 1.91 and 1.72 eV for NCO, d-NCRO and n-NCRO (with the theoretical overpotentials of 0.75, 0.68 and 0.49 V), respectively, indicating the better OER activity of d-NCRO and n-NCRO than that of NCO.

To give insight into the enhanced OER activity of d-NCRO and n-NCRO, the *d* band center (ε_d) of the Co *d* orbitals of NCO and Ru *d* orbitals of d-NCRO and n-NCRO were calculated. As shown in Fig. 5d, the ε_d for the surface Co *d* orbitals of NCO is − 1.59 eV, while the ε_d for the surface Ru *d* orbitals of d-NCRO and n-NCRO is − 2.31 and − 2.11 eV, respectively. The decrease of the ε_d will lead to the weakening of the binding strength of some reaction intermediates (such as *OH and *OOH) [53], resulting in the more optimal binding strength of the reaction intermediates and better OER activities on d-NCRO and n-NCRO as compared to that on NCO [54]. We further plot the value of ΔG_O-ΔG_{OH} (a descriptor for the activity of the OER of various materials) as a function of the calculated ε_d [8]. A good linear relation can be obtained as shown in Fig. 5e, indicating that the enhanced OER activity of d-NCRO and n-NCRO can indeed be ascribed to the variation of the energy level of the *d* band center.

4. Conclusions

In summary, we developed an outstanding bifunctional NCRO electrocatalyst by a combination of bulk (Ru-doping) and surface (Ru nanoparticles) modification of NCO for overall water splitting at high current density. The detailed characterizations and DFT calculations revealed that the strong synergetic electron coupling between Ru and NCO, which originated from both Ru doping in bulk NCO and followed Ru nanoparticles modification on NCO surface, can mainly boost the activity and stability for HER, OER, and overall water splitting. Moreover, it can reduce the energy barrier in both Volmer and Tafel step and optimized the adsorption energy of reaction intermediates. For HER, the NCRO-4 requires only 138 mV overpotential to achieve 1000 mA cm^{-2}, as well as 420 mV at 1500 mA cm^{-2} for OER, eventually, an electrolyzer using NCRO-4 as both cathode and anode could be established that it only need 1.45 V cell voltage to attain 10 mA cm^{-2}. The performance is comparable to that of all the reported catalysts so far. The proposed NCRO electrocatalyst should serve as a model for simple dual modification of spinel or other metal-based materials for efficient overall water splitting at high current density.

CRediT authorship contribution statement

Dewen Wang: Investigation, Data curation, Resources, Writing – original draft, Writing – review & editing. **Yuting Chen**: Investigation, Software, Formal analysis, Resources, Writing – original draft. **Libin Fan**: Investigation, Formal analysis, Resources. **Ting Xiao**: Software, Formal analysis. **Tian Meng**: Software, Resources. **Zhicai Xing**: Conceptualization, Methodology, Resources, Writing – original draft, Writing – review & editing, Funding acquisition, Supervision. **Xiurong Yang**: Writing – review & editing, Funding acquisition, Supervision.

Declaration of Competing Interest

The authors declare that they have no known competing financial interests or personal relationships that could have appeared to influence the work reported in this paper.

Acknowledgments

This work was supported by the National Natural Science Foundation of China (No. 22034006 and 21721003), Key Research Program of Frontier Sciences, Chinese Academy of Sciences (No. QYZDY-SSW-SLH019) and the Development Project of Science and Technology of Jilin Province (No. 20200201074JC).

Appendix A. Supporting information

Supplementary data associated with this article can be found in the online version at doi:10.1016/j.apcatb.2022.121081.

References

[1] M.S. Dresselhaus, I.L. Thomas, Alternative energy technologies, Nature 414 (2001) 332–337.
[2] B. Dunn, H. Kamath, J.M. Tarascon, Electrical energy storage for the grid: a battery of choices, Science 334 (2011) 928–935.
[3] H.A. Gasteiger, N.M. Marković, Just a dream—or future reality? Science 324 (2009) 48–49.
[4] Z. Zhuang, Y. Wang, C.Q. Xu, S. Liu, C. Chen, Q. Peng, Z. Zhuang, H. Xiao, Y. Pan, S. Lu, R. Yu, W.C. Cheong, X. Cao, K. Wu, K. Sun, Y. Wang, D. Wang, J. Li, Y. Li, Three-dimensional open nano-netcage electrocatalysts for efficient pH-universal overall water splitting, Nat. Commun. 10 (2019) 4875.
[5] B. Tang, X. Yang, Z. Kang, L. Feng, Crystallized $RuTe_2$ as unexpected bifunctional catalyst for overall water splitting, Appl. Catal. B Environ. 278 (2020), 119281.
[6] D. Wang, Q. Li, C. Han, Q. Lu, Z. Xing, X. Yang, Atomic and electronic modulation of self-supported nickel-vanadium layered double hydroxide to accelerate water splitting kinetics, Nat. Commun. 10 (2019) 3899.
[7] X. Zou, Y. Zhang, Noble metal-free hydrogen evolution catalysts for water splitting, Chem. Soc. Rev. 44 (2015) 5148–5180.
[8] Z.W. Seh, J. Kibsgaard, C.F. Dickens, I. Chorkendorff, J.K. Nørskov, T.F. Jaramillo, Combining theory and experiment in electrocatalysis: insights into materials design, Science 355 (2017) eaad4998.
[9] D. Song, D. Hong, Y. Kwon, H. Kim, J. Shin, H.M. Lee, E. Cho, Highly porous Ni–P electrode synthesized by an ultrafast electrodeposition process for efficient overall water electrolysis, J. Mater. Chem. A 8 (2020) 12069–12079.
[10] Y. Jiao, Y. Zheng, M. Jaroniec, S.Z. Qiao, Design of electrocatalysts for oxygen- and hydrogen-involving energy conversion reactions, Chem. Soc. Rev. 44 (2015) 2060–2086.
[11] B. You, Y. Sun, Innovative strategies for electrocatalytic water splitting, Acc. Chem. Res. 51 (2018) 1571–1580.
[12] N.C.S. Selvam, L. Du, B. Xia, P.J. Yoo, B. You, Reconstructured water oxidation electrocatalysts: the impact of surface dynamics on intrinsic activities, Adv. Funct. Mater. 31 (2021), 2008190.
[13] B. You, Y. Sun, Hierarchically porous nickel sulfide multifunctional superstructures, Adv. Energy Mater. 6 (2016), 1502333.
[14] A. Buttler, H. Spliethoff, Current status of water electrolysis for energy storage, grid balancing and sector coupling via power-to-gas and power-to-liquids: a review, Renew. Sustain. Energy Rev. 82 (2018) 2440–2454.
[15] B. Zhong, P. Kuang, L. Wang, J. Yu, Hierarchical porous nickel supported NiFeOxHy nanosheets for efficient and robust oxygen evolution electrocatalyst under industrial condition, Appl. Catal. B Environ. 299 (2021), 120668.

[16] Y. Jin, H. Wang, J. Li, X. Yue, Y. Han, P.K. Shen, Y. Cui, Porous MoO_2 nanosheets as non-noble bifunctional electrocatalysts for overall water splitting, Adv. Mater. 28 (2016) 3785–3790.
[17] Y. Liu, X. Luo, C. Zhou, S. Du, D. Zhen, B. Chen, J. Li, Q. Wu, Y. Iru, D. Chen, A modulated electronic state strategy designed to integrate active HER and OER components as hybrid heterostructures for efficient overall water splitting, Appl. Catal. B Environ. 260 (2020), 118197.
[18] Y. Wu, Y. Liu, G.D. Li, X. Zou, X. Lian, D. Wang, L. Sun, T. Asefa, X. Zou, Efficient electrocatalysis of overall water splitting by ultrasmall $Ni_xCo_{3-x}S_4$ coupled Ni_3S_2 nanosheet arrays, Nano Energy 35 (2017) 161–170.
[19] Q. Zhao, Z. Yan, C. Chen, J. Chen, Spinels: controlled preparation, oxygen reduction/evolution reaction application, and beyond, Chem. Rev. 117 (2017) 10121–10211.
[20] X. Gao, H. Zhang, Q. Li, X. Yu, Z. Hong, X. Zhang, C. Liang, Z. Lin, Hierarchical $NiCo_2O_4$ hollow microcuboids as bifunctional electrocatalysts for overall water-splitting, Angew. Chem. Int. Ed. 55 (2016) 6290–6294.
[21] G. Zhang, X.W. Lou, General solution growth of mesoporous $NiCo_2O_4$ nanosheets on various conductive substrates as high-performance electrodes for supercapacitors, Adv. Mater. 25 (2013) 976–979.
[22] Y. Li, P. Hasin, Y. Wu, $Ni_xCo_{3-x}O_4$ nanowire arrays for electrocatalytic oxygen evolution, Adv. Mater. 22 (2010) 1926–1929.
[23] J. Song, C. Wei, Z.F. Huang, C. Liu, L. Zeng, X. Wang, Z.J. Xu, A review on fundamentals for designing oxygen evolution electrocatalysts, Chem. Soc. Rev. 49 (2020) 2196–2214.
[24] S. Sun, Y. Sun, Y. Zhou, S. Xi, X. Ren, B. Huang, H. Liao, L.P. Wang, Y. Du, Z.J. Xu, Shifting oxygen charge towards octahedral metal: a way to promote water oxidation on cobalt spinel oxides, Angew. Chem. Int. Ed. 58 (2019) 6042–6047.
[25] Z. Peng, D. Jia, A.M. Al-Enizi, A.A. Elzatahry, G. Zheng, From water oxidation to reduction: homologous Ni–Co based nanowires as complementary water splitting electrocatalysts, Adv. Energy Mater. 5 (2015), 1402031.
[26] J. Bao, X. Zhang, B. Fan, J. Zhang, M. Zhou, W. Yang, X. Hu, H. Wang, B. Pan, Y. Xie, Ultrathin spinel-structured nanosheets rich in oxygen deficiencies for enhanced electrocatalytic water oxidation, Angew. Chem. Int. Ed. 54 (2015) 7399–7404.
[27] J. Wang, W. Fang, Y. Hu, Y. Zhang, J. Dang, Y. Wu, B. Chen, H. Zhao, Z. Li, Single atom Ru doping 2H-MoS_2 as highly efficient hydrogen evolution reaction electrocatalyst in a wide pH range, Appl. Catal. B Environ. 298 (2021), 120490.
[28] X. Xiao, X. Wang, X. Jiang, S. Song, D. Huang, L. Yu, Y. Zhang, S. Chen, M. Wang, Y. Shen, Z. Ren, In situ growth of Ru nanoparticles on $(Fe,Ni)(OH)_2$ to boost hydrogen evolution activity at high current density in alkaline media, Small Methods 4 (2020), 1900796.
[29] C.B. Hong, X. Li, W.B. Wei, X.T. Wu, Q.L. Zhu, Nano-engineering of Ru-based hierarchical porous nanoreactors for highly efficient pH-universal overall water splitting, Appl. Catal. B Environ. 294 (2021), 120230.
[30] J. Yu, Q. He, G. Yang, W. Zhou, Z. Shao, M. Ni, Recent advances and prospective in ruthenium-based materials for electrochemical water splitting, ACS Catal. 9 (2019) 9973–10011.
[31] Y. Zheng, Y. Jiao, Y. Zhu, L.H. Li, Y. Han, Y. Chen, M. Jaroniec, S.Z. Qiao, High electrocatalytic hydrogen evolution activity of an anomalous ruthenium catalyst, J. Am. Chem. Soc. 138 (2016) 16174–16181.
[32] R. Subbaraman, D. Tripkovic, D. Strmcnik, K.C. Chang, M. Uchimura, A. P. Paulikas, V. Stamenkovic, N.M. Markovic, Enhancing hydrogen evolution activity in water splitting by tailoring Li^+-$Ni(OH)_2$-Pt interfaces, Science 334 (2011) 1256–1260.
[33] Q. Wu, M. Luo, J. Han, W. Peng, Y. Zhao, D. Chen, M. Peng, J. Liu, F.M.F. de Groot, Y. Tan, Identifying electrocatalytic sites of the nanoporous copper–ruthenium alloy for hydrogen evolution reaction in alkaline electrolyte, ACS Energy Lett. 5 (2020) 192–199.
[34] M. Li, H. Wang, W. Zhu, W. Li, C. Wang, X. Lu, RuNi nanoparticles embedded in N-doped carbon nanofibers as a robust bifunctional catalyst for efficient overall water splitting, Adv. Sci. 7 (2020), 1901833.
[35] P. Li, M. Wang, X. Duan, L. Zheng, X. Cheng, Y. Zhang, Y. Kuang, Y. Li, Q. Ma, Z. Feng, W. Liu, X. Sun, Boosting oxygen evolution of single-atomic ruthenium through electronic coupling with cobaltiron layered double hydroxides, Nat. Commun. 10 (2019) 1711.
[36] X. Chen, J. Wang, J. Wang, Q. Zhang, L. Gu, L. Zheng, N. Wang, R. Yu, Atomically dispersed ruthenium on nickel hydroxide ultrathin nanoribbons for highly efficient hydrogen evolution reaction in alkaline media, Adv. Mater. 33 (2021), 2104764.
[37] L. Fang, Z. Jiang, H. Xu, L. Liu, Y. guan, X. Gu, Y. Wang, Crystal-plane engineering of $NiCo_2O_4$ electrocatalysts towards efficient overall water splitting, J. Catal. 357 (2018) 238–246.
[38] X. Zhang, R. Sa, S. Yang, F. Zhou, Z. Jiang, R. Wang, A non-carbon catalyst support upgrades the intrinsic activity of ruthenium for hydrogen evolution electrocatalysis via strong interfacial electronic effects, Nano Energy 75 (2020), 104981.
[39] Y. Liu, Y. Ying, L. Fei, Y. Liu, Q. Hu, G. Zhang, S.Y. Pang, W. Lu, C.L. Mak, X. Luo, L. Zhou, M. Wei, H. Huang, Valence engineering via selective atomic substitution on tetrahedral sites in spinel oxide for highly enhanced oxygen evolution catalysis, J. Am. Chem. Soc. 141 (2019) 8136–8145.
[40] J. Ge, D. Zhang, Y. Qin, T. Dou, M. Jiang, F. Zhang, X. Lei, Dual-metallic single Ru and Ni atoms decoration of MoS_2 for high-efficiency hydrogen production, Appl. Catal. B Environ. 298 (2021), 120557.
[41] M.C. Biesinger, B.P. Payne, A.P. Grosvenor, L.W.M. Lau, A.R. Gerson, R.S.C. Smart, Resolving surface chemical states in XPS analysis of first row transition metals, oxides and hydroxides: Cr, Mn, Fe, Co and Ni, Appl. Surf. Sci. 257 (2011) 2717–2730.
[42] L. Shen, Q. Che, H. Li, X. Zhang, Mesoporous $NiCo_2O_4$ nanowire arrays grown on carbon textiles as binder-free flexible electrodes for energy storage, Adv. Funct. Mater. 24 (2014) 2630–2637.
[43] Y. Qiao, S. Guo, K. Zhu, P. Liu, X. Li, K. Jiang, C.J. Sun, M. Chen, H. Zhou, Reversible anionic redox activity in Na_3RuO_4 cathodes: a prototype Na-rich layered oxide, Energy Environ. Sci. 11 (2018) 299–305.
[44] L. Zhu, S. Shan, V. Petkov, W. Hu, A. Kroner, J. Zheng, C. Yu, N. Zhang, Y. Li, R. Luque, C.J. Zhong, H. Ye, Z. Yang, B.H. Chen, Ruthenium–nickel–nickel hydroxide nanoparticles for room temperature catalytic hydrogenation, J. Mater. Chem. A 5 (2017) 7869–7875.
[45] J. He, W. Li, P. Xu, J. Sun, Tuning electron correlations of RuO_2 by co-doping of Mo and Ce for boosting electrocatalytic water oxidation in acidic media, Appl. Catal. B Environ. 298 (2021), 120528.
[46] J. Yang, H. Liu, W.N. Martens, R.L. Frost, Synthesis and characterization of cobalt hydroxide, cobalt oxyhydroxide, and cobalt oxide nanodiscs, J. Phys. Chem. C 114 (2010) 111–119.
[47] X. Cui, P. Ren, C. Ma, J. Zhao, R. Chen, S. Chen, N.P. Rajan, H. Li, L. Yu, Z. Tian, D. Deng, Robust interface Ru centers for high-performance acidic oxygen evolution, Adv. Mater. 32 (2020), 1908126.
[48] T. Wang, J. Wang, Y. Sun, Y. Duan, S. Sun, X. Hu, S. Xi, Y. Du, C. Wang, Z. Xu, Origin of electronic structure dependent activity of spinel $ZnNi_xCo_{2-x}O_4$ oxides for complete methane oxidation, Appl. Catal. B Environ. 256 (2019), 117844.
[49] T. Wang, Y. Sun, Y. Zhou, S. Sun, X. Hu, Y. Dai, S. Xi, Y. Du, Y. Yang, Z. Xu, Identifying influential parameters of octahedrally coordinated cations in spinel $ZnMn_xCo_{2-x}O_4$ oxides for the oxidation reaction, ACS Catal. 8 (2018) 8568–8577.
[50] X. Wang, X. Peng, H. Ran, B. Lin, J. Ni, J. Lin, L. Jiang, Influence of Ru substitution on the properties of $LaCoO_3$ catalysts for ammonia synthesis: XAFS and XPS studies, Ind. Eng. Chem. Res. 57 (2018) 17375–17383.
[51] Z. Chen, X. Duan, W. Wei, S. Wang, B.J. Ni, Recent advances in transition metal-based electrocatalysts for alkaline hydrogen evolution, J. Mater. Chem. A 7 (2019) 14971–15005.
[52] C.G. Morales Guio, L.A. Stern, X. Hu, Nanostructured hydrotreating catalysts for electrochemical hydrogen evolution, Chem. Soc. Rev. 43 (2014) 6555–6569.
[53] C. Ling, L. Shi, Y. Ouyang, X.C. Zeng, J. Wang, Nanosheet supported single-metal atom bifunctional catalyst for overall water splitting, Nano Lett. 17 (2017) 5133–5139.
[54] J. Greeley, T.F. Jaramillo, J. Bonde, I. Chorkendorff, J.K. Nørskov, Computational high-throughput screening of electrocatalytic materials for hydrogen evolution, Nat. Mater. 5 (2006) 909–913.

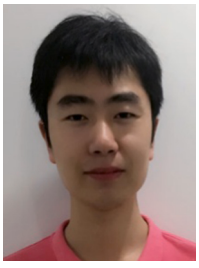

Dewen Wang obtained his B.S. degree in 2015 from Qingdao University of Science and Technology, China. Currently, he is pursuing his Ph.D. degree under the supervision of Prof. Xiurong Yang in Changchun Institute of Applied Chemistry, Chinese Academy of Sciences. His research focuses on the preparation and characterization of noble metal-free electrocatalysts for hydrogen evolution reaction.

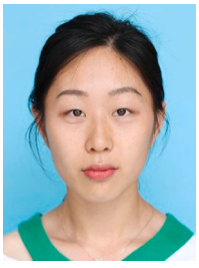

Yuting Chen obtained her B.S. degree in 2019 from Anhui Normal University. Currently, she is pursuing her Ph.D. degree under the supervision of Prof. Xiurong Yang in Changchun Institute of Applied Chemistry, Chinese Academy of Sciences. Her research focuses on the design and regulation of transition metal based catalysts and their applications in catalysis and electro-catalysis.

Libing Fan is currently a Ph.D. candidate at College of Chemistry, Jilin University. She received her Bachelor's degree from Zhengzhou Normal University in 2015 and Master's degree from Changchun University of Science and Technology in 2018. Her research interests focus on the metal-based carbon composites for hydrogen and oxygen evolution reaction.

Ting Xiao obtained her B.S. degree in 2015 from Hainan University, China. Currently, she is pursuing her Ph.D. degree under the supervision of Prof. Xiurong Yang in Changchun Institute of Applied Chemistry, Chinese Academy of Sciences. Her research focuses on design and synthesis of new functional materials with various compositions and morphologies via chemical and physical processes for biomolecules interaction and biosensing.

Tian Meng is pursuing a Ph.D. degree from Changchun Institute of Applied Chemistry, Chinese Academy of Sciences, under the supervision of Prof. Xiurong Yang. He obtained his B.S. degree in Material Science from Wuhan University of Technology in 2014. His research interests focus on metal organic frameworks and corresponding applications in catalysis and analytic detection.

Zhicai Xing is an associate professor of the State Key Laboratory of Electroanalytical Chemistry, Changchun Institute of Applied Chemistry, Chinese Academy of Sciences. His current research interests focus on the developing rational strategies for chemical synthesis, assembly and integration of nanomaterials, investigating the fundamental synthesis-structure-property relationships by creatively and synergistically integrating our combination of expertise in both synthetic materials chemistry and nanoscience and nanotechnology, and finally applying these advanced materials for biological sensing, energy storage and electrocatalysis applications.

Xiurong Yang is a professor of the State Key Laboratory of Electroanalytical Chemistry, Changchun Institute of Applied Chemistry, Chinese Academy of Sciences. Her current research mainly focuses on design and synthesis of new functional materials with various compositions and morphologies via chemical and physical processes for biomolecules interaction, biosensing and energy storage applications.